RESEARCH ARTICLE

Figures and figure supplements

Structural and biophysical analysis of a *Haemophilus influenzae* tripartite ATP-independent periplasmic (TRAP) transporter

Michael J Currie and James S Davies *et al*.

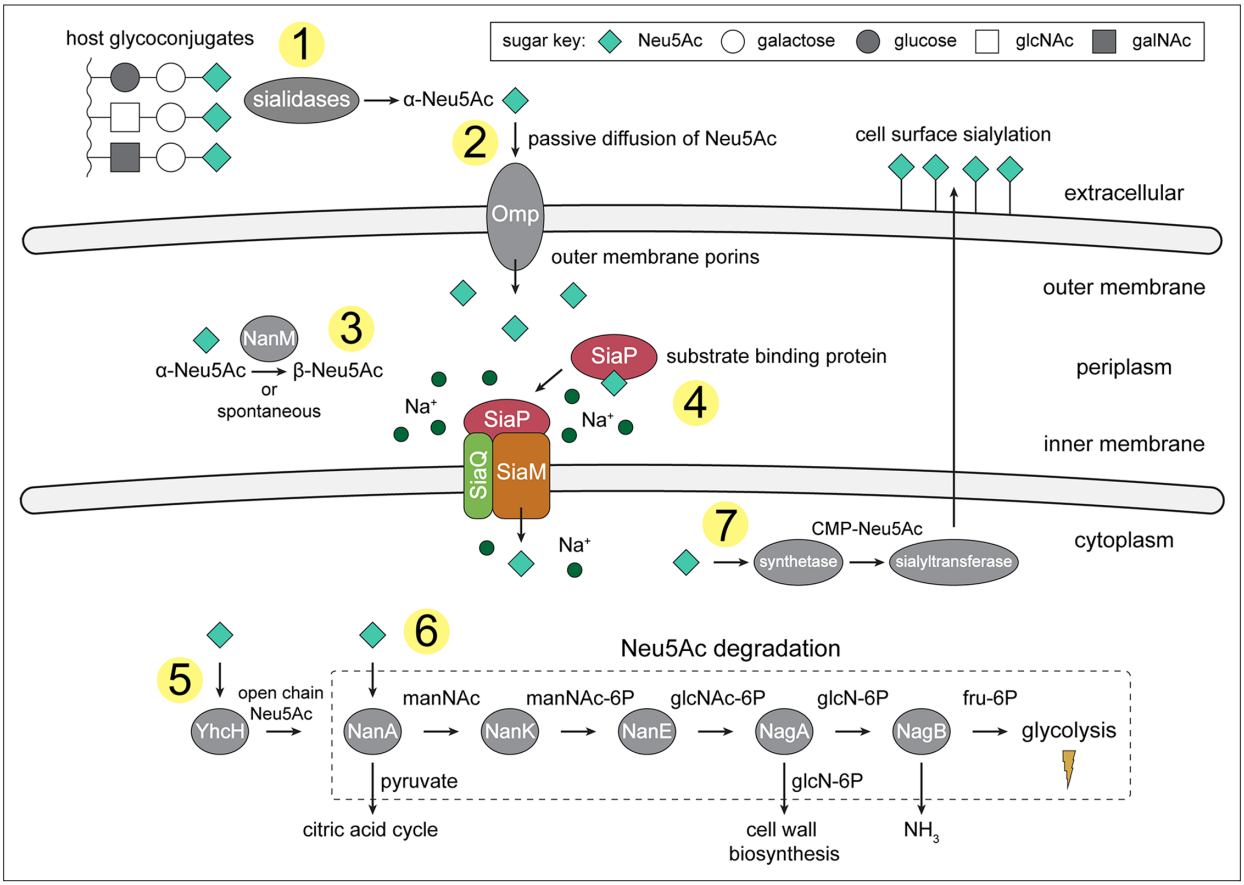

Figure 1. An overview of Neu5Ac metabolism in *H. influenzae*. (1) *H. influenzae* is sialidase negative and relies on environmental sialidases to hydrolyse and release terminal Neu5Ac from human glycoconjugates. (2) Outer membrane porins facilitate diffusion of Neu5Ac into the periplasm. (3) A mutarotase, NanM, catalyses the formation of β-Neu5Ac from α-Neu5Ac to prepare for active transport across the inner membrane. (4) Neu5Ac is captured by the high-affinity substrate-binding protein, SiaP. SiaP delivers Neu5Ac to the SiaQM TRAP transporter, which uses a Na^+ electrochemical gradient to drive transport. *H. influenzae* cannot synthesise Neu5Ac and relies solely on SiaPQM for obtaining environmental Neu5Ac. (5) Cytoplasmic processing of Neu5Ac by an anomerase, YhcH, generates the unfavourable open chain form in preparation for use by the first enzyme of the Neu5Ac degradation pathway, NanA. (6) Neu5Ac is sequentially degraded into cell wall constituents or fructose-6-phosphate, which can enter glycolysis. Five conserved enzymes (an aldolase, NanA; kinase, NanK; epimerase, NanE; deacetylase, NagA; and deaminase, NagB) are involved in this pathway which provides *H. influenzae* with carbon, nitrogen, and energy. (7) Alternatively, Neu5Ac can be activated by cytidine monophosphate and a sialic acid synthetase and added to lipooligosaccharides by a sialyltransferase. Neu5Ac, *N*-acetylneuraminate; manNAc, *N*-acetylmannosamine; manNAc-6P, *N*-acetylmannosamine-6-phosphate; glcNAc, *N*-acetylglucosamine; glcNAc-6P, *N*-acetylglucosamine-6-phosphate; glcN-6P, glucosamine-6-phosphate; fru-6P, fructose-6-phosphate; galNAc, *N*-acetylgalactosamine; CMP, cytidine monophosphate; Omp, outer membrane porin; NanM, Neu5Ac mutarotase; YhcH, Neu5Ac anomerase; NanA, Neu5Ac lyase; NanK, manNAc kinase; NanE, manNAc-6P epimerase; NagA, glcNAc-6P deacetylase; NagB, glcN-6P deaminase.

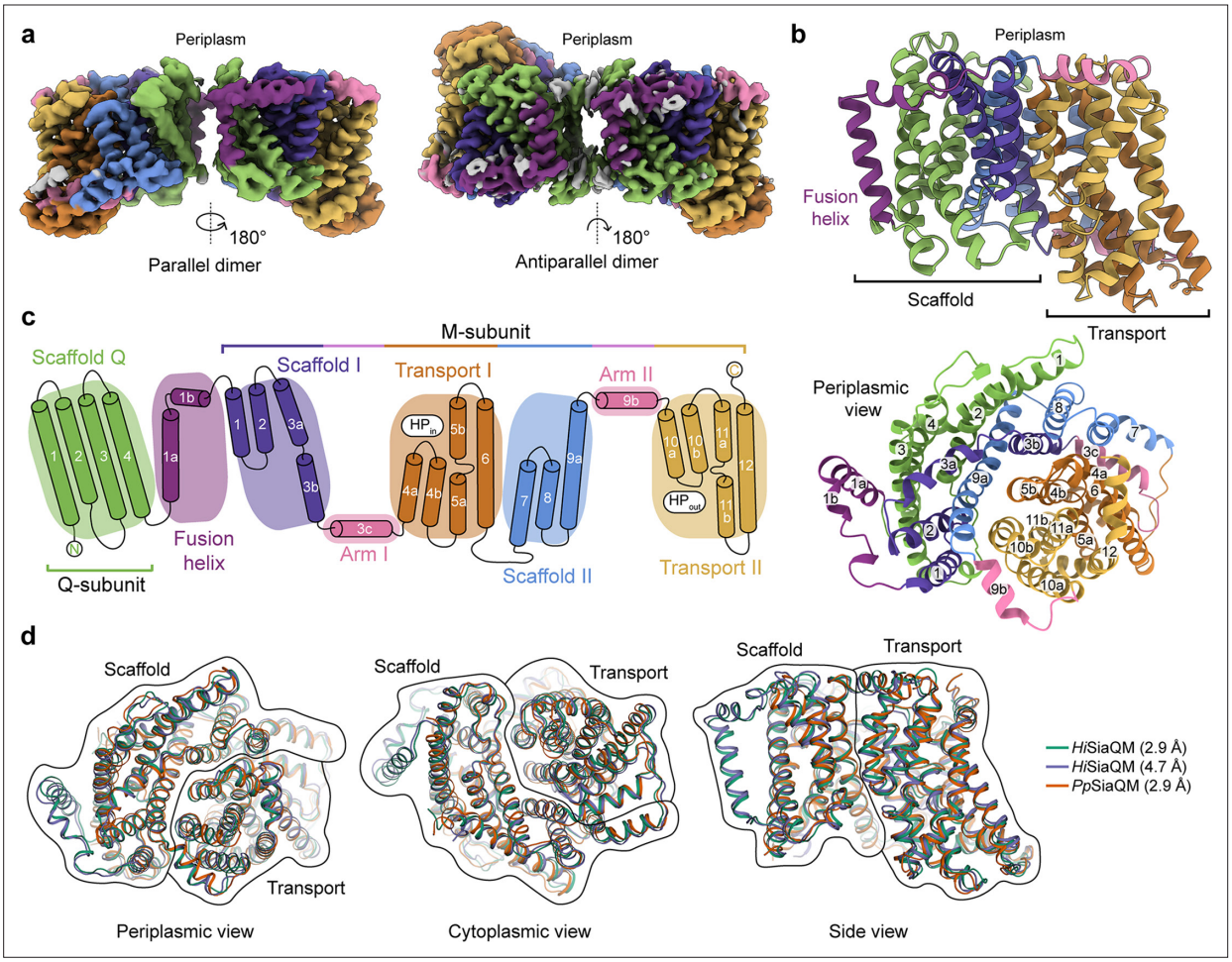

Figure 2. The structure of *Hi*SiaQM. (**a**) Coulomb maps for the parallel (3.36 Å) and antiparallel (2.99 Å) *Hi*SiaQM homodimers. The periplasmic surfaces of the monomers are facing the same direction for the parallel dimer (PDB: 8THI), whereas the periplasmic surface of one monomer is rotated 180° for the antiparallel dimer (PDB: 8THJ). The transport domain (orange and gold) is in the 'elevator down' conformation in all four monomers. The dimeric interface in both maps is distanced and neither has significant protein–protein interactions. The maps are coloured according to the topology in (**c**). Density consistent with phospholipids is coloured grey and is particularly present in the dimer interface of the higher resolution antiparallel dimer map. (**b**) Structural model of the *Hi*SiaQM monomer. The transport domain is in the 'elevator down' conformation with the substrate-binding site facing the cytoplasm. (**c**) The topology of *Hi*SiaQM is the same as the non-fused *Pp*SiaQM with the addition of the fusion helix. The M-subunit forms the transport domain (orange and gold) and bracing arm helices (pink) as well as a large portion of the scaffold (purple and blue). The Q-subunit is entirely used as a scaffold for the elevator transport mechanism. The fusion helix (purple) connects the scaffold and adds to its size. It also forms a short horizontal helix, similar to the arm helices of the M-subunit. (**d**) A structural overlay of *Hi*SiaQM (2.9 Å structure, green; 4.7 Å structure, purple) and *Pp*SiaQM (2.9 Å structure, orange) shows that the helices of the structures are well aligned, and all three structures are in the same conformation.

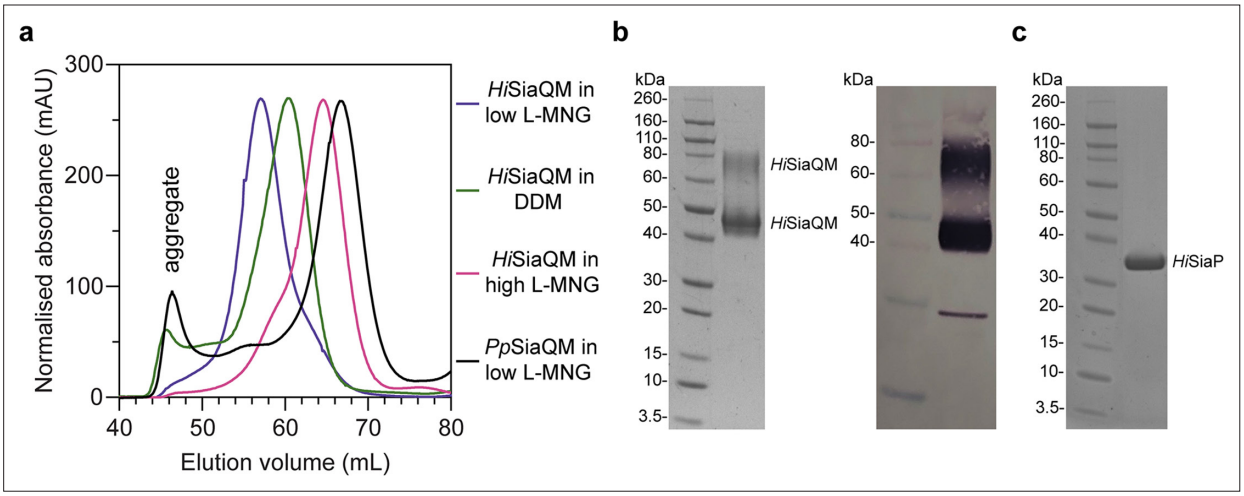

Figure 2—figure supplement 1. Size-exclusion chromatography traces of SiaQM transporters suggests that *Hi*SiaQM exists as multiple species in detergent. (**a**) *Hi*SiaQM purified in dodecyl-β-D-maltoside (DDM) (green trace) results in significant aggregation at 45–50 mL, which is not apparent when solubilised in lauryl maltose neopentyl glycol (L-MNG) (blue and pink traces). *Hi*SiaQM purified in a low concentration of L-MNG (blue trace) results in a higher order species with a peak at 57 mL compared to *Hi*SiaQM purified in a high concentration of L-MNG (pink trace), which has a peak at 65 mL. At a similar protein concentration (~5 mg/mL) in DDM, *Hi*SiaQM elutes as a single peak between these volumes at 60 mL (green trace). For comparison, non-fused SiaQM from *P. profundum* expressed with the same purification tag and purified in a low concentration of L-MNG (black trace) has a dominant peak at 67 mL, characteristic of a monomer, and this greatly contrasts against *Hi*SiaQM in low L-MNG (blue trace). (**b**) SDS-PAGE gel (left) of L-MNG purified *Hi*SiaQM that consistently ran as two bands (~45 and ~75 kDa). Protein of this purity (>95%) in L-MNG was used for all subsequent experiments, including for further reconstitution into amphipol or nanodiscs. Western blot (right) with anti-Xpress primary antibody identifies both large bands that appear on SDS-PAGE following purification to be *Hi*SiaQM. A small amount of a lower molecular weight contaminant or degradation product was also present. (**c**) SDS-PAGE gel demonstrating the purity of *Hi*SiaP. A single band at ~35 kDa indicates that *Hi*SiaP is greater than 95% pure. Protein of this purity (>95%) was used for all subsequent experiments.

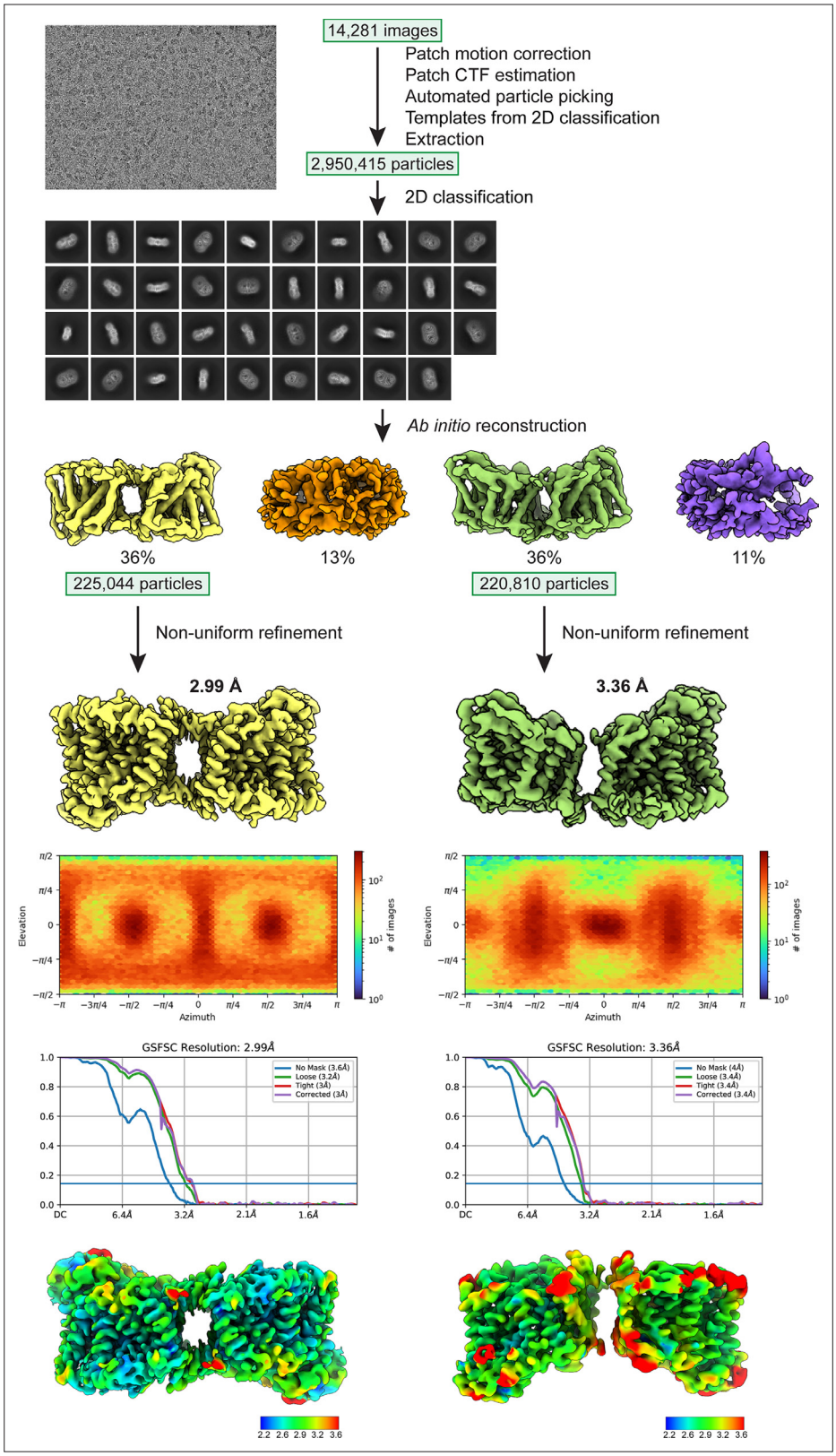

Figure 2—figure supplement 2. Cryo-electron microscopy (cryo-EM) workflow for structure determination. The two classes were determined as 36% of the particles (antiparallel dimer) and 36% (parallel dimer).

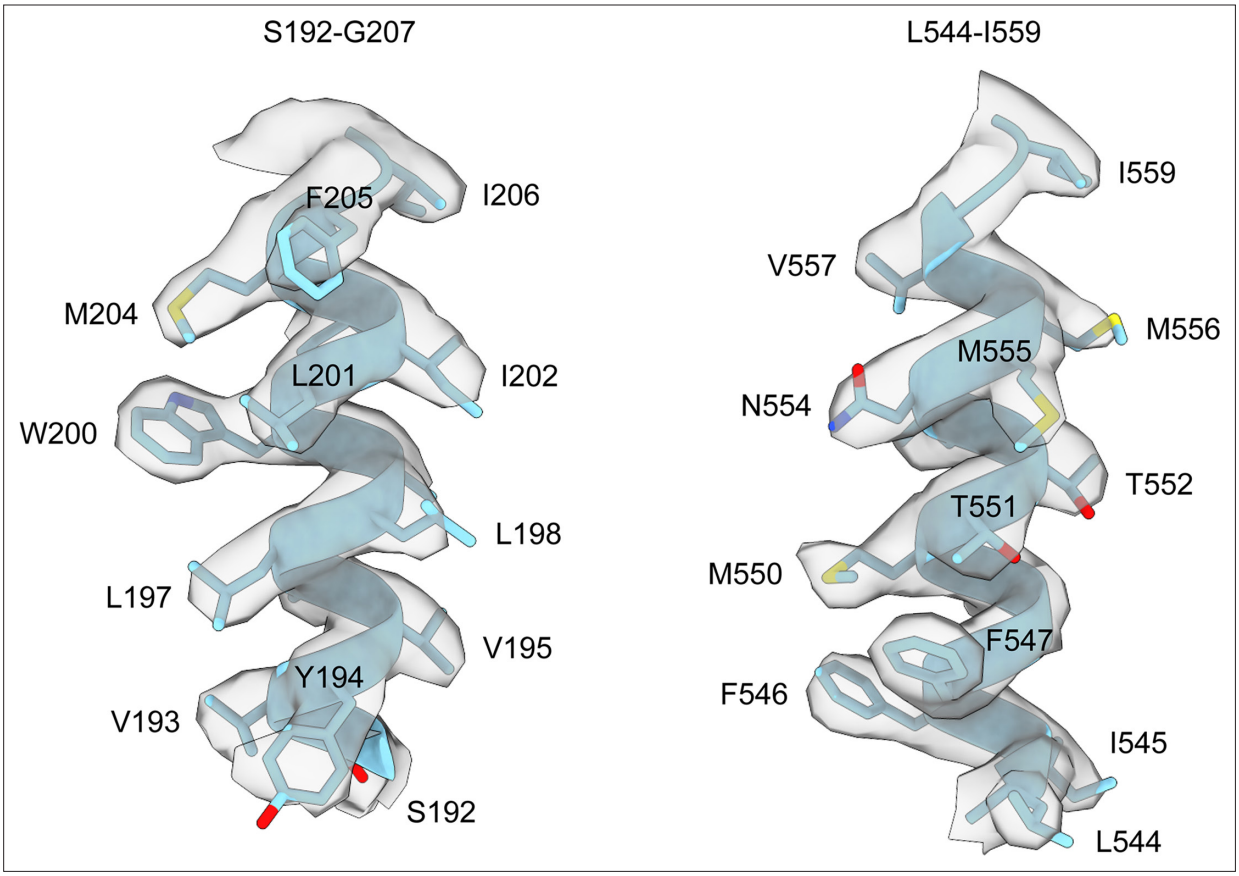

Figure 2—figure supplement 3. Representative density of the helices of *Hi*SiaQM. Clear side-chain densities are present for almost all of the residues of *Hi*SiaQM. Density for the antiparallel dimer is shown as it is higher resolution and was used for the structural analysis in this work.

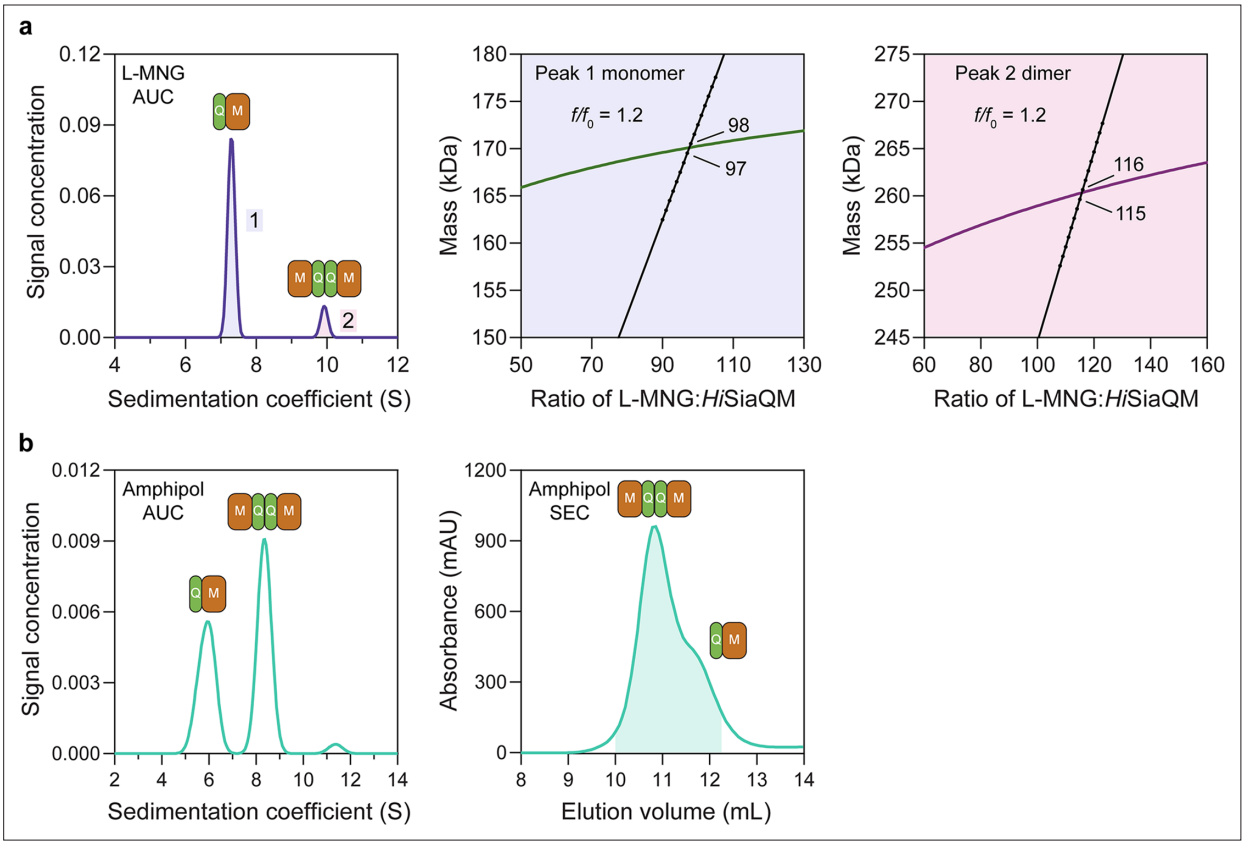

Figure 3. *Hi*SiaQM self-association in lauryl maltose neopentyl glycol (L-MNG) and amphipol. (**a**) Sedimentation velocity analytical ultracentrifugation (SV-AUC) analysis of *Hi*SiaQM in L-MNG (left panel). Two well-resolved species exist at 7.3S (diffusion coefficient, D = 4.8 × 10^{-7} cm^2/s) and 9.9S (D = 4.2 × 10^{-7} cm^2/s), with the larger peak constituting 85% of the signal. The species at 7.3S (peak 1, blue shading) is most consistent with *Hi*SiaQM as a monomer with ~98 molecules of L-MNG bound (middle panel; green = measured mass, black = theoretical mass), calculated from the experimental sedimentation and diffusion coefficients. These calculations suggest that peak 1 existing as a dimer is unlikely, as the dimeric protein would only have ~14 molecules of L-MNG bound. Additionally, the calculated f/f_0 of a monomer for peak 1 is 1.2, consistent with a protein in a detergent micelle. The species at 9.9S (peak 2, pink shading) is most consistent with *Hi*SiaQM as a dimer with ~116 molecules of L-MNG bound (calculated) (right panel; purple = measured mass, black = theoretical mass); peak 2 existing as a monomer is not possible, as the protein clearly has a smaller species in peak 1 and cannot be divided further than a monomer, and a trimer is also unlikely as the trimeric protein would only have ~32 molecules of L-MNG bound (calculated). Additionally, the calculated f/f_0 of a dimer for peak 2 is also 1.2, again consistent with a protein in a detergent micelle. These calculations do not account for bound lipid molecules. (**b**) Left panel: SV-AUC analysis of amphipol-solubilised *Hi*SiaQM (initially purified in L-MNG) shows two distinct species present at 5.9S and 8.3S. These are monomeric and dimeric species as L-MNG-solubilised protein exists as these oligomeric states at 7.3S and 9.9S as in (**a**). Right panel: representative size-exclusion chromatogram of amphipol-solubilised *Hi*SiaQM favouring the dimeric state. The main peak at ~10.8 mL contains dimeric *Hi*SiaQM and the shoulder at ~11.8 mL contains monomeric *Hi*SiaQM. The sample used for structure determination is shaded turquoise.

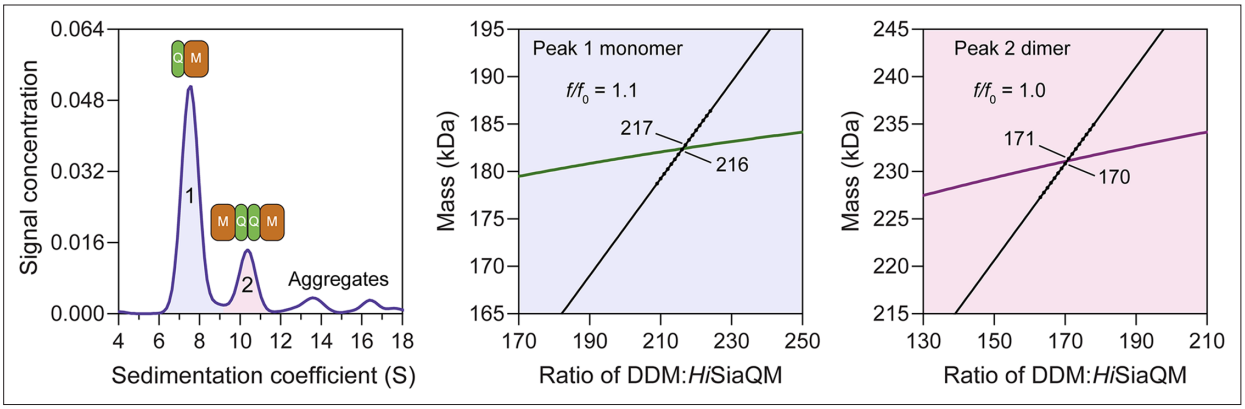

Figure 3—figure supplement 1. *Hi*SiaQM self-association in dodecyl-β-d-maltoside (DDM). Sedimentation velocity analytical ultracentrifugation (SV-AUC) analysis of *Hi*SiaQM in DDM (left panel). Two well-resolved species exist at 7.6S (diffusion coefficient, D = 5.0 × 10^{-7} cm^2/s) and 10.3S (D = 5.0 × 10^{-7} cm^2/s), with the larger peak constituting 62% of the signal. Due to the presence of protein aggregation in DDM (***Figure 2—figure supplement 1a***, green trace), SV-AUC for this sample was performed at 4°C (instead of 20°C for lauryl maltose neopentyl glycol [L-MNG]) to prevent *Hi*SiaQM from forming larger order species, although even at this temperature larger species are still evident at 12–18S and extend to ~40S (not shown). This observed heterogeneity was a significant reason for our use of L-MNG in all other experiments. The species at 7.6S (peak 1, blue shading) is most consistent with *Hi*SiaQM as a monomer with ~216 molecules of DDM bound (middle panel; green = measured mass, black = theoretical mass), calculated from the experimental sedimentation and diffusion coefficients. These calculations suggest that peak 1 existing as a dimer is unlikely, as the dimeric protein would only have ~31 molecules of DDM bound. Additionally, the calculated f/f_0 of a monomer for peak 1 is 1.1, consistent with a protein in a detergent micelle. The species at 10.3S (peak 2, pink shading) is most consistent with *Hi*SiaQM as a dimer with ~171 molecules of DDM bound (calculated) (right panel; purple = measured mass, black = theoretical mass); peak 2 existing as a monomer is not possible as the protein clearly has a smaller species in peak 1 and cannot be divided further than a monomer, and a trimer is also unlikely as the experimental data suggests that no DDM would be bound (calculated). Additionally, the calculated f/f_0 of a dimer for peak 2 is 1.0, roughly consistent with a protein in a detergent micelle. These calculations do not account for bound lipid molecules.

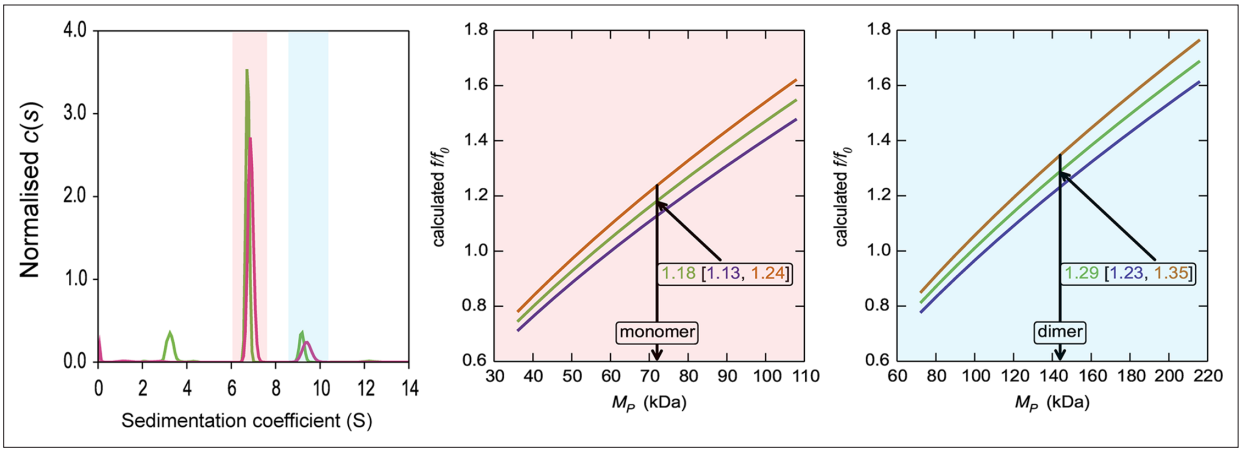

Figure 3—figure supplement 2. *Hi*SiaQM self-association in lauryl maltose neopentyl glycol (L-MNG) (interference analysis). Sedimentation of *Hi*SiaQM in L-MNG (left panel) with absorbance data (pink) and interference data (green). Two well-resolved species exist at 6.7S and 9.4S, with the smaller species constituting greater than 80% of the signal. The oligomeric state of the two species was verified using the membrane protein calculations function of GUSSI (***Brautigam, 2015***), as described previously (***Ebel, 2011***; ***le Maire et al., 2008***; ***Le Roy et al., 2015***; ***Salvay et al., 2007***). Free L-MNG micelles are seen only with interference data at ~3.2S. The peak at 6.7S is most consistent with a *Hi*SiaQM monomer (middle panel). After determining the amount of L-MNG bound to the protein with the interference data, frictional ratios (f/f_0) can be calculated to test the hypothesised oligomeric state. The calculated f/f_0 for a monomer for the major species (red shading) is 1.2 (1σ error = 1.13–1.24), consistent with a single *Hi*SiaQM in a detergent micelle. A dimer is unlikely since the calculated f/f_0 for a dimer for the major species is 1.9 (1σ error = 1.79–1.96) (not shown). On the right panel, the calculated f/f_0 for a dimer for the minor species (blue shading) is 1.3 (1σ error = 1.23–1.35), again consistent with dimeric *Hi*SiaQM in a detergent micelle. A monomer is unlikely, since the calculated f/f_0 for a monomer for the 9.4S species is 0.8 (1σ error = 0.78–0.85) (not shown). With the detergent bound to the sedimenting protein now known alongside the mass of the detergent monomers, it can be estimated that approximately 90 (monomer) and 150 (dimer) molecules of L-MNG are bound to the protein.

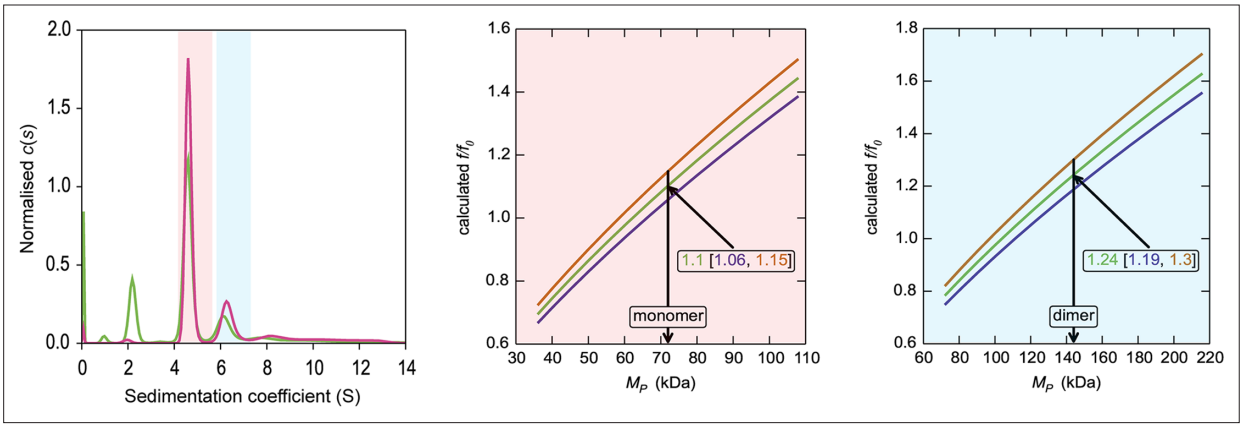

Figure 3—figure supplement 3. *Hi*SiaQM self-association in dodecyl-β-D-maltoside (DDM) (interference analysis). Sedimentation of *Hi*SiaQM in DDM (left panel) with absorbance data (pink) and interference data (green). Two main species exist at ~4.5S and ~6.2S, with the smaller species constituting greater than 60% of the signal. The oligomeric state of the two species was verified using the membrane protein calculations function of GUSSI (***Brautigam, 2015***), as described previously (***Ebel, 2011***; ***le Maire et al., 2008***; ***Le Roy et al., 2015***; ***Salvay et al., 2007***). Free DDM micelles are seen only with interference data at ~2.1S. Due to the presence of protein aggregation in DDM (***Figure 2—figure supplement 1a***, green trace), sedimentation velocity analytical ultracentrifugation (SV-AUC) for this sample was performed at 4°C (instead of 20°C for the sample in lauryl maltose neopentyl glycol [L-MNG]) to prevent the protein from forming larger order species, although even at this temperature some larger species are still evident at ~8–12S. These sedimentation coefficients are not corrected for the lower temperature so appear smaller than all other values reported for *Hi*SiaQM. The species at 4.5S (red shading) is consistent with a monomer in DDM, f/f_0 = 1.1 (1σ error = 1.06–1.15) (middle panel). In contrast, a dimer species is unlikely given the unrealistic f/f_0 = 1.8 (1σ error = 1.68–1.82) (not shown). The larger species at 6.5S (blue shading) is consistent with a dimer in DDM, f/f_0 = 1.2 (1σ error = 1.19–1.3) (right panel), whereas the monomer provides an unrealistic f/f_0 = 0.8 (1σ error = 0.75–0.82) (not shown). With the detergent bound to the sedimenting protein now known alongside the mass of the detergent monomers, it can be estimated that approximately 220 (monomer) and 380 (dimer) molecules of DDM are bound to the protein.

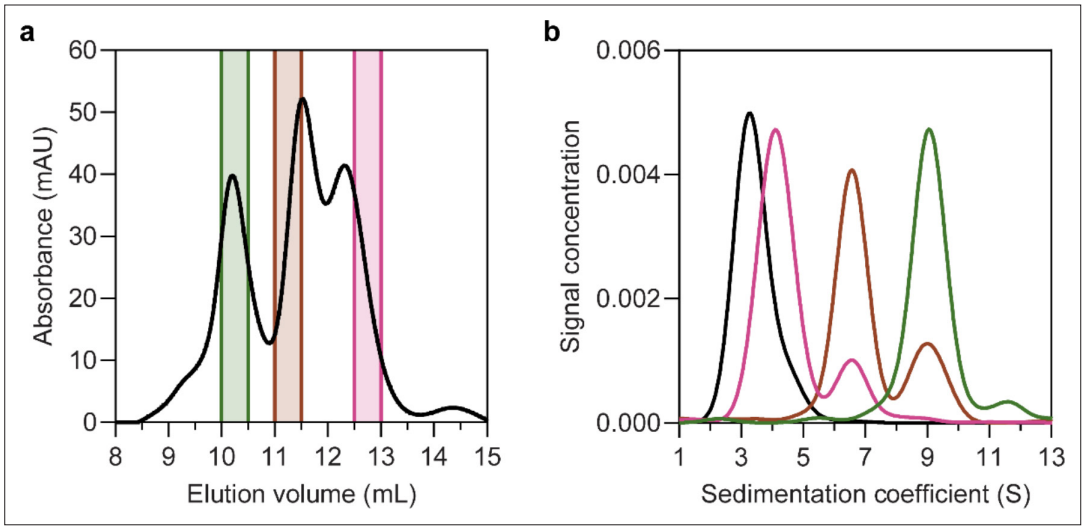

Figure 3—figure supplement 4. Solubilisation of *Hi*SiaQM in nanodiscs. (**a**) The size-exclusion chromatogram following nanodisc reconstitution with a 1:4:80 ratio of *Hi*SiaQM:MSP:lipid identifies the presence of multiple species. Three fractions across the elution profile were analysed with sedimentation velocity analytical ultracentrifugation (SV-AUC) (shown by the coloured bars). (**b**) SV-AUC analysis of nanodisc solubilised *Hi*SiaQM (pink, brown, and green) and empty nanodiscs (black) shows that later eluted fractions gave a main species consistent with empty nanodiscs (pink, 4.0S), middle eluted fractions gave a main species consistent with a monomer incorporated (brown, 6.8S) and earlier eluted fractions gave a larger 9.0S main species (green). The larger species at 9.0S is most likely a dimer of *Hi*SiaQM in a nanodisc as it has been shown to exist as a dimer in both detergent and amphipol. The dimer can just fit by physical constraints as the MSP forms ~11 nm nanodiscs and the size of the *Hi*SiaQM dimer is ~10 nm at the widest point. While physically possible, the number of reconstituted lipids would be low.

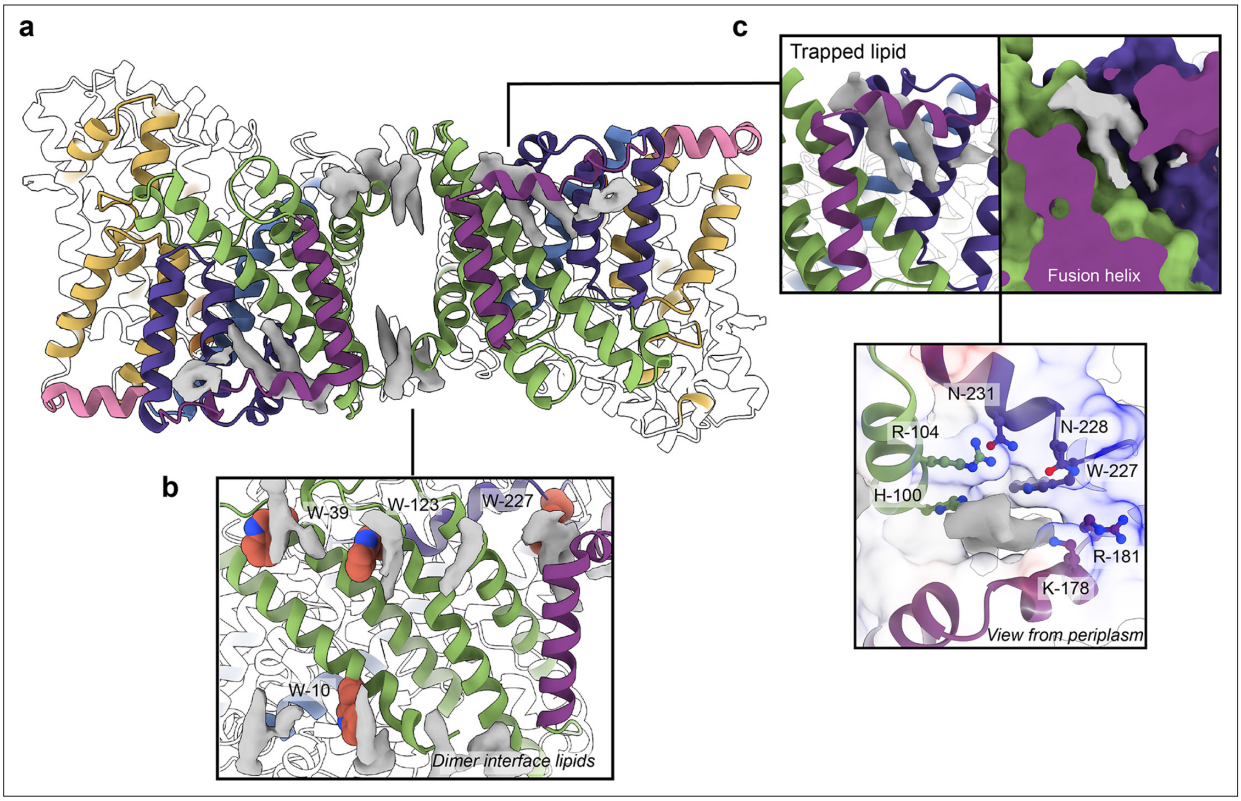

Figure 4. Phospholipids bound to *Hi*SiaQM. (**a**) The dimer has well-defined areas of density (grey) that correspond to bound phospholipids. Two mechanistically important areas are the dimer interface and fusion helix pocket. (**b**) Phospholipids are present at the dimer interface, including in close contact with the anchoring tryptophan residues (shown as spheres) of the Q-subunits that provide stability to the scaffold domain. (**c**) A single phospholipid is trapped in a pocket formed by the fusion helix (protein model surface shown in colour, EM density in grey). The lipid is on the periplasmic side of the transporter and the headgroup appears to be coordinated by residues surrounding the top of the pocket, which have a generally positive character.

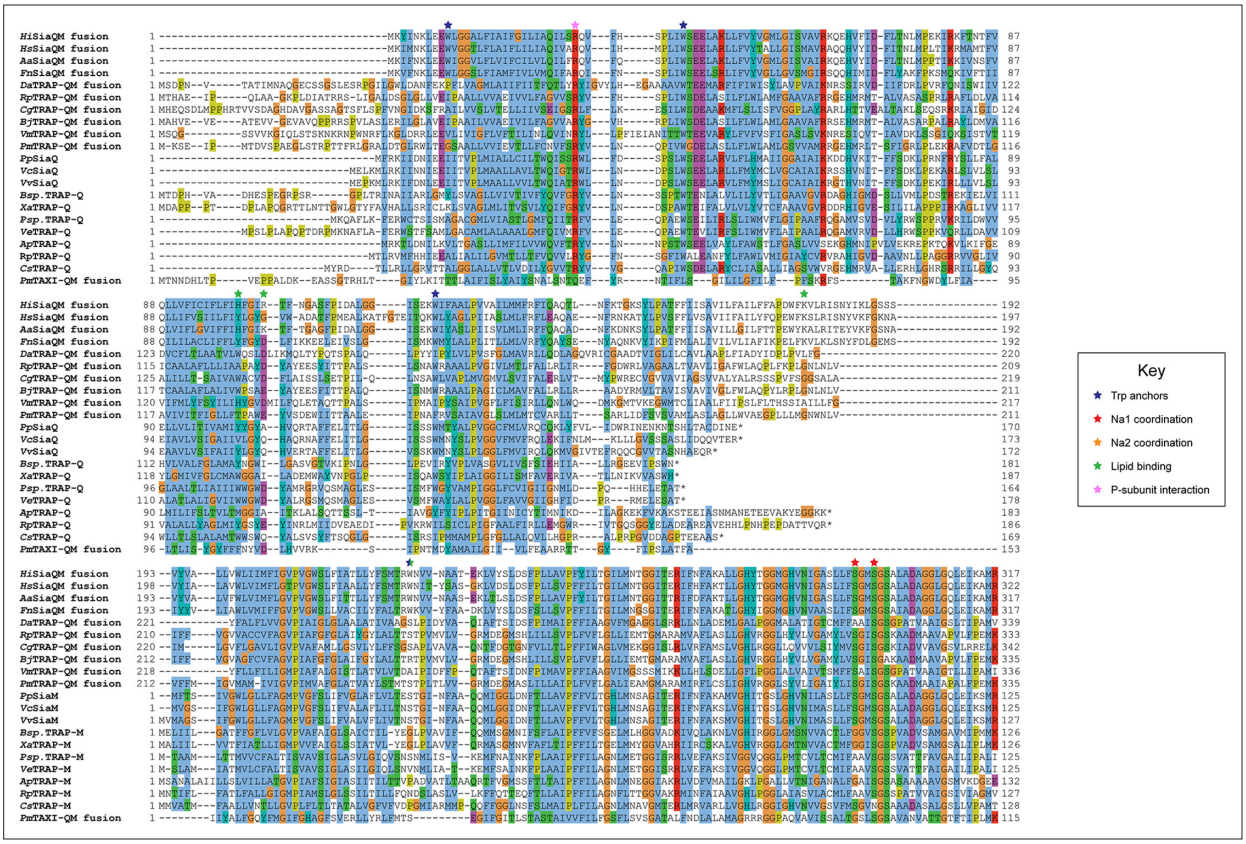

Figure 4—figure supplement 1. Protein sequence alignment of tripartite ATP-independent periplasmic (TRAP) transporter QM-subunits. Protein sequences were obtained from the National Center for Biotechnology Information, aligned using Kalign (***Lassmann, 2019***) and coloured in Jalview (***Waterhouse et al., 2009***) with Clustal X colouring. Anchoring tryptophan residues (blue stars), Na1 coordinating residues (red stars), Na2 coordinating residues (orange stars), predicted lipid-binding residues (green stars), and expected P-subunit interacting residues (pink stars) are annotated. SiaQM protein sequences from *Haemophilus influenzae* (*Hi*, WP_005694432), *Histophilus somni* (*Hs*, WP_249962964), *Aggregatibacter actinomycetemcomitans* (*Aa*, WP_005592763), *Fusobacterium nucleatum* (*Fn*, WP_060798477), *Photobacterium profundum* (*Pp*, WP_011218955/WP_011218954), *Vibrio vulnificus* (*Vv*, WP_001889698/WP_000233105), and *Vibrio cholerae* (*Vc*, WP_011081661/BAC97226) were aligned with TRAP-QM protein sequences from *Desulfovibrio alaskensis* (*Da*, WP_011367273), *Rhodopseudomonas palustris* (*Rp*, WP_011441572), *Caballeronia grimmiae* (*Cg*, WP_052006082), *Bradyrhizobium japonicum* (*Bj*, WP_248883330), *Virgibacillus massiliensis* (*Vm*, WP_051739028), *Pseudomonas mandelii* (*Pm*, WP_033060252), *Bradyrhizobium* sp. BTAi1 (*Bsp.*, WP_011942649/WP_011942650), *Xanthobacter autotrophicus* (*Xa*, ABS68596/ABS68595), *Polaromonas* sp. JS666 (*Psp.*, WP_011482802/WP_011482801), *Verminephrobacter eiseniae* (*Ve*, ABM59662/WP_011811650), *Anaerococcus prevotii* (*Ap*, WP_015778303/WP_015778302), *Rhodopseudomonas palustris* (*Rp*, WP_011442208/WP_011442207), and *Chromohalobacter salexigens* (*Cs*, WP_011505968/ABE58023) and the TAXI-TRAP-QM protein sequence from *Proteus mirabilis* (*Pm*, WP_004242632).

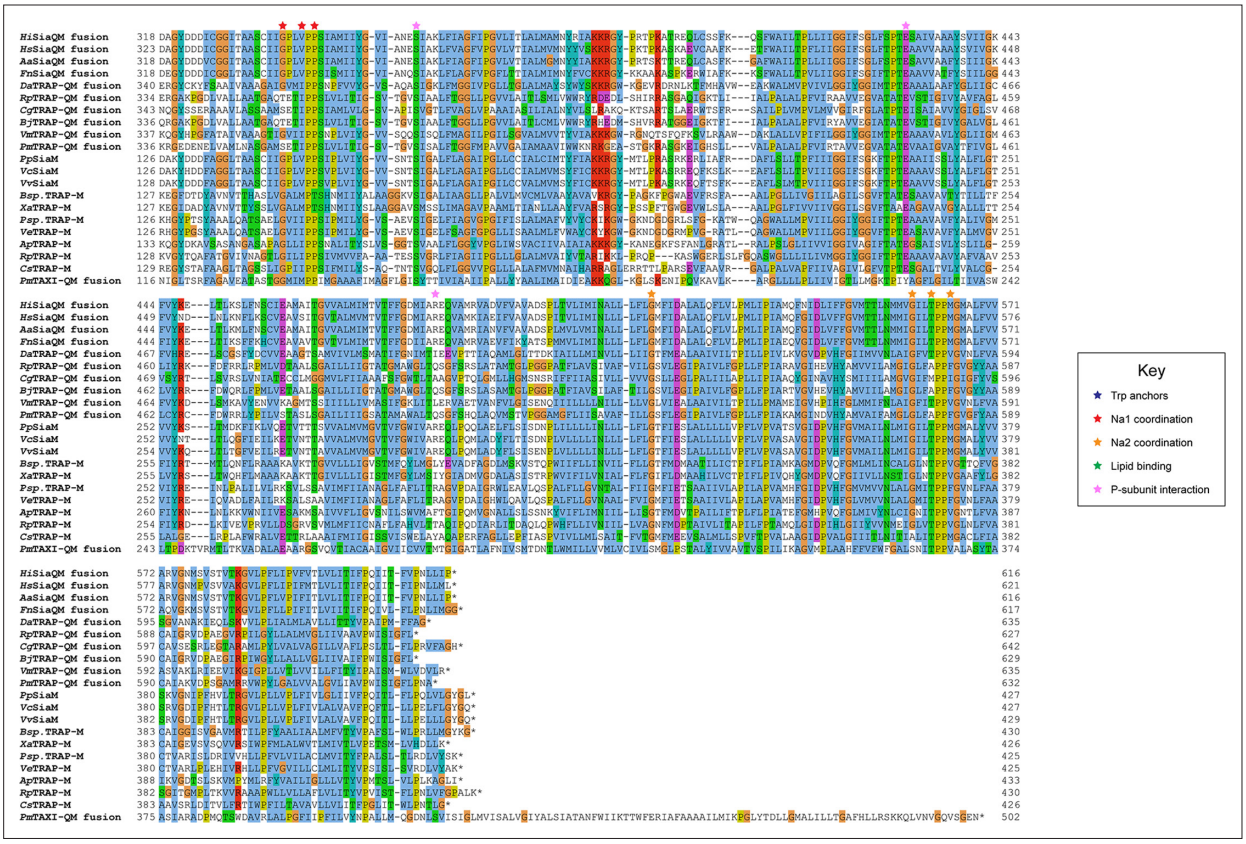

Figure 4—figure supplement 2. Protein sequence alignment of tripartite ATP-independent periplasmic (TRAP) transporter QM-subunits. Protein sequences were obtained from the National Center for Biotechnology Information, aligned using Kalign (***Lassmann, 2019***) and coloured in Jalview (***Waterhouse et al., 2009***) with Clustal X colouring. Anchoring tryptophan residues (blue stars), Na1 coordinating residues (red stars), Na2 coordinating residues (orange stars), predicted-lipid binding residues (green stars), and expected P-subunit interacting residues (pink stars) are annotated. SiaQM protein sequences from *Haemophilus influenzae* (*Hi*, WP_005694432), *Histophilus somni* (*Hs*, WP_249962964), *Aggregatibacter actinomycetemcomitans* (*Aa*, WP_005592763), *Fusobacterium nucleatum* (*Fn*, WP_060798477), *Photobacterium profundum* (*Pp*, WP_011218955/WP_011218954), *Vibrio vulnificus* (*Vv*, WP_001889698/WP_000233105), and *Vibrio cholerae* (*Vc*, WP_011081661/BAC97226) were aligned with TRAP-QM protein sequences from *Desulfovibrio alaskensis* (*Da*, WP_011367273), *Rhodopseudomonas palustris* (*Rp*, WP_011441572), *Caballeronia grimmiae* (*Cg*, WP_052006082), *Bradyrhizobium japonicum* (*Bj*, WP_248883330), *Virgibacillus massiliensis* (*Vm*, WP_051739028), *Pseudomonas mandelii* (*Pm*, WP_033060252), *Bradyrhizobium* sp. BTAi1 (*Bsp.*, WP_011942649/WP_011942650), *Xanthobacter autotrophicus* (*Xa*, ABS68596/ABS68595), *Polaromonas* sp. JS666 (*Psp.*, WP_011482802/WP_011482801), *Verminephrobacter eiseniae* (*Ve*, ABM59662/WP_011811650), *Anaerococcus prevotii* (*Ap*, WP_015778303/WP_015778302), *Rhodopseudomonas palustris* (*Rp*, WP_011442208/WP_011442207), and *Chromohalobacter salexigens* (*Cs*, WP_011505968/ABE58023) and the TAXI-TRAP-QM protein sequence from *Proteus mirabilis* (*Pm*, WP_004242632).

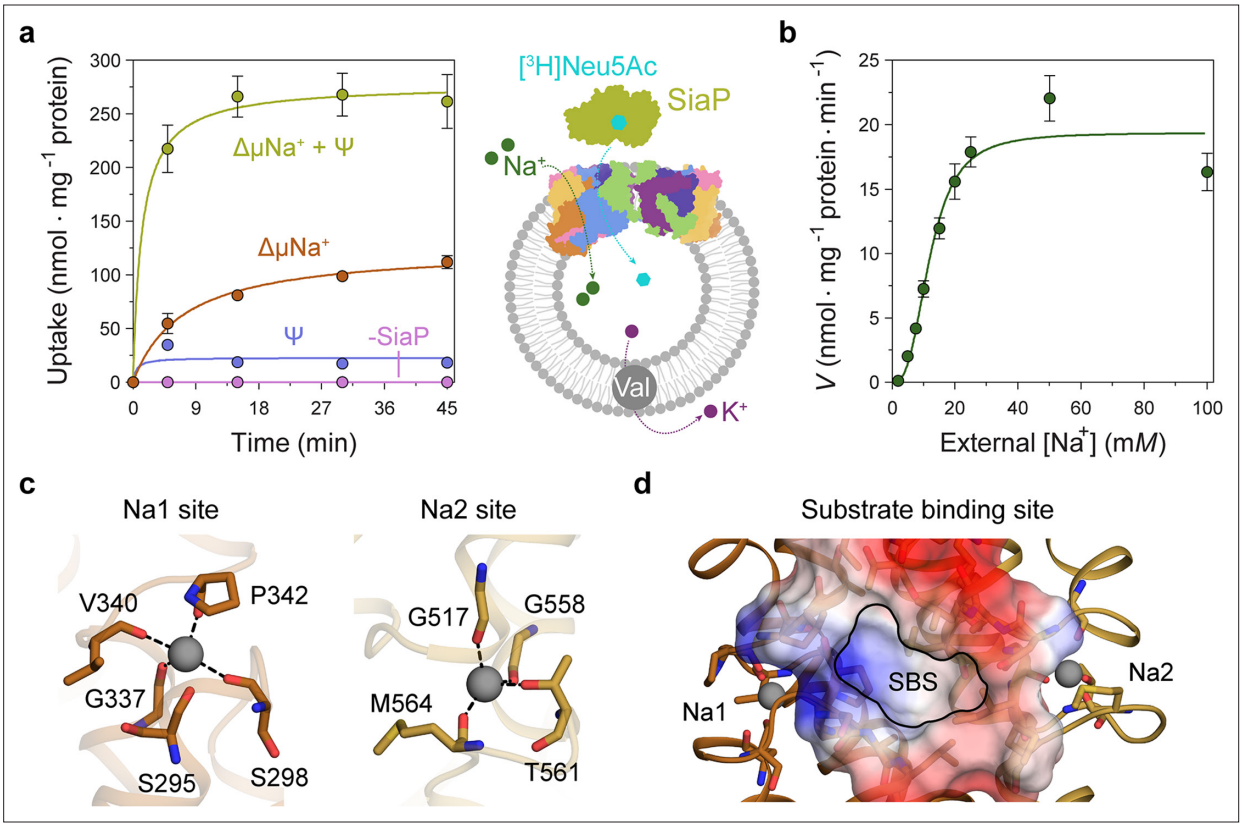

Figure 5. Transport assays demonstrate that lauryl maltose neopentyl glycol (L-MNG)-solubilised *Hi*SiaQM is functional. (**a**) [^{3}H]-Neu5Ac uptake was measured at multiple time intervals under each condition and used to calculate transport rates. *Hi*SiaQM had the highest activity in the presence of *Hi*SiaP, a membrane potential and a Na^+ gradient (green circles). Approximately one-third of this rate was present without a membrane potential (orange circles). Transport was low in the absence of Na^+ (blue circles) and negligible without *Hi*SiaP (pink circles). Error bars represent the standard error of the mean (SEM) for three technical replicates, except without *Hi*SiaP, which has two replicates. The assay diagram contains the parallel *Hi*SiaQM structure, coloured by topology as in ***Figure 2a and c***. This is for visual presentation; it is not known if the transporter exists as a dimeric species in the assay. (**b**) The rate of transport is dependent on the concentration of Na^+, showing a sigmoidal response (Hill coefficient = 2.9 [95% C.I. 2.2–3.9]). The K_M for Na^+ is 12 mM (95% C.I. 10–14 mM). The displayed response shows that *Hi*SiaPQM operates close to its maximum measured rate at a reasonably low external Na^+ concentration (25 mM). Error bars represent the SEM of five technical replicates. (**c**) Two Na^+-binding sites (Na1 and Na2) were identified in *Hi*SiaQM. These sites share highly similar coordinating residues with *Pp*SiaQM. At the Na1 site, a Na^+ ion (grey) is coordinated by the carbonyl groups of S298, G337, V340 and P342 (orange sticks, coordination shown as black dashes). S295 is also shown but its carbonyl is positioned just outside the coordination distance in our structure. At the Na2 site, a Na^+ ion (grey) is coordinated by the carbonyl groups of G517, G558, and M564, and the side-chain hydroxyl of T561 (gold sticks, coordination shown as black dashes). (**d**) A putative substrate-binding site (SBS, outlined) is located in the transport domain of *Hi*SiaQM (orange and gold). The mostly hydrophobic binding site (shown as sticks and electrostatic surface) exists between the two Na^+-binding sites and is large enough to bind Neu5Ac.

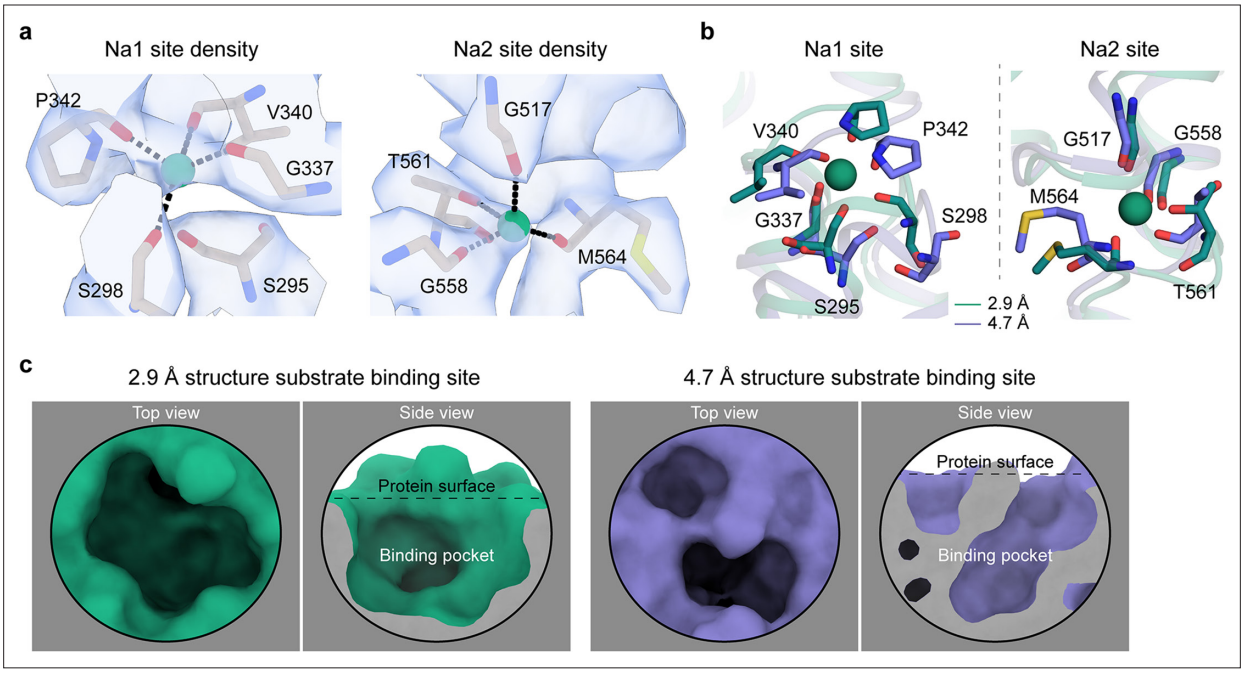

Figure 5—figure supplement 1. The Na^+ and substrate-binding sites of *Hi*SiaQM. (**a**) Closeup views of the cryo-electron microscopy (cryo-EM) density (blue) at the Na1 and Na2 sites of the antiparallel *Hi*SiaQM dimer. Density is present for both Na^+ ions (green spheres). Na^+-binding residues are shown as sticks and Na^+ coordination as black dashes. The density map was automatically sharpened using Phenix (***Terwilliger et al., 2018***) and the radii of the Na^+ ions have been reduced to show the density more clearly. (**b**) A comparison of the Na^+-binding sites of *Hi*SiaQM from the 2.9 Å structure (green) and the 4.7 Å structure (purple). The Na^+ ions of the 2.9 Å structure are shown as green spheres and are well positioned to coordinate the identified binding residues in the 'clamshell' loops. The positions of these loops are different between the two structures. (**c**) A comparison of the putative Neu5Ac-binding sites of *Hi*SiaQM from the 2.9 Å structure (green) and the 4.7 Å structure (purple). The higher resolution structure shows that a defined binding pocket exists at the centre of the transport domain.

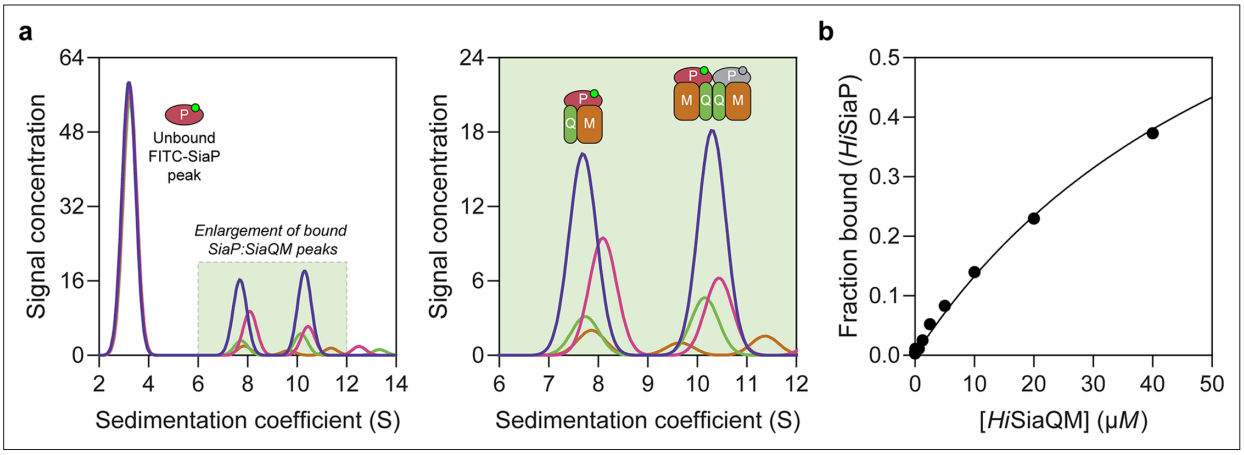

Figure 6. Sedimentation velocity analytical ultracentrifugation (AUC) analysis of the interaction between *Hi*SiaQM and *Hi*SiaP in lauryl maltose neopentyl glycol (L-MNG) detergent. (**a**) Titrating increasing concentrations of *Hi*SiaQM (blue, 40 μM [2.88 mg/mL]; pink, 20 μM; green, 10 μM; brown, 5 μM; other concentrations omitted for clarity) against fluorescently labelled FITC-*Hi*SiaP (10 nM) identifies a shift in the signal for *Hi*SiaP from 3S to ~7.5S and ~10.5S. This shift demonstrates binding to *Hi*SiaQM and identifies two bound species with different sedimentation coefficients. The two species are annotated with the most likely binding stoichiometries (one or two *Hi*SiaP monomers [red and grey] may be binding the dimeric species). (**b**) Fitting a binding model to the data (fraction bound = $[P]_{total}/([P]_{total} + K_D)$ estimates a K_D of 65 μM (95% C.I. = 62–69 μM, $R^2 = 0.99$).

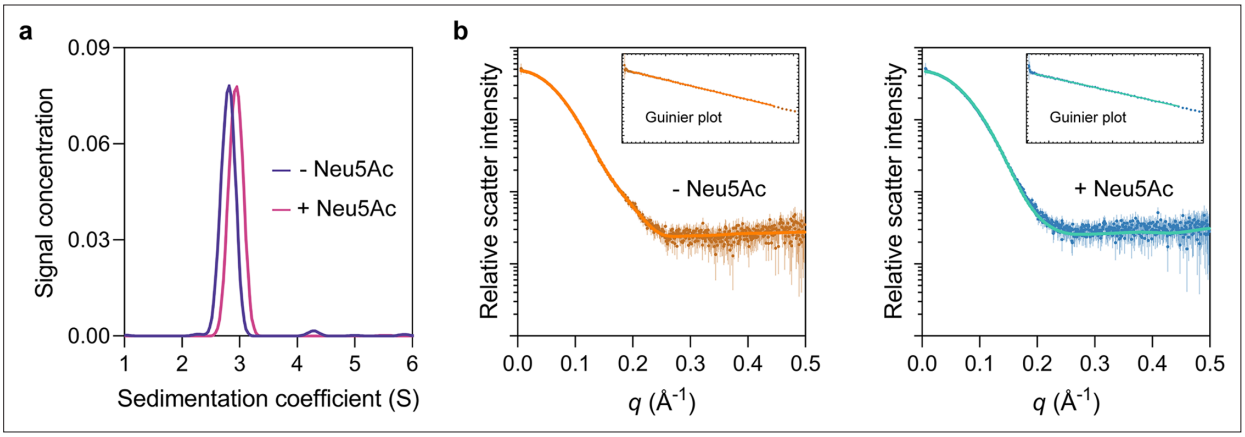

Figure 6—figure supplement 1. *Hi*SiaP is monomeric. (**a**) Analytical ultracentrifugation experiments of *Hi*SiaP (expressed in the periplasm) without Neu5Ac or with 5 mM Neu5Ac resulted in sedimentation coefficients of ~2.8S without Neu5Ac (blue) and ~3.0S with Neu5Ac (pink), consistent with a monomeric oligomeric state. The samples had calculated masses of 39 and 35 kDa, indicating that *Hi*SiaP exists as a monomer in both a ligand bound and unbound state. (**b**) Small-angle X-ray scattering (SAXS) analysis of *Hi*SiaP without Neu5Ac (left, brown) and with 5 mM Neu5Ac (right, blue) at a considerably higher protein concentration than analytical ultracentrifugation (360 µM) resulted in a radius of gyration (R_g) of 20.9 Å and a maximum particle dimension (D_{max}) of 64 Å without Neu5Ac and 20 Å and 63 Å with 5 mM Neu5Ac. CRYSOL was used to fit the predicted scatter from monomeric crystal structures to the observed scatter (***Manalastas-Cantos et al., 2021***). Fitting *Hi*SiaP without Neu5Ac (PDB: 2CEY) (left, orange) results in χ^2 = 0.32. Fitting *Hi*SiaP with Neu5Ac (PDB: 3B50) (right, teal) results in χ^2 = 0.66. Fitting the incorrect structures results in χ^2 values of 4.91 (without Neu5Ac data to 3B50) and 2.36 (with Neu5Ac data to 2CEY). These SAXS analyses of *Hi*SiaP are all consistent with the sizes of the monomers from crystallography (***Müller et al., 2006***; ***Johnston et al., 2008***).

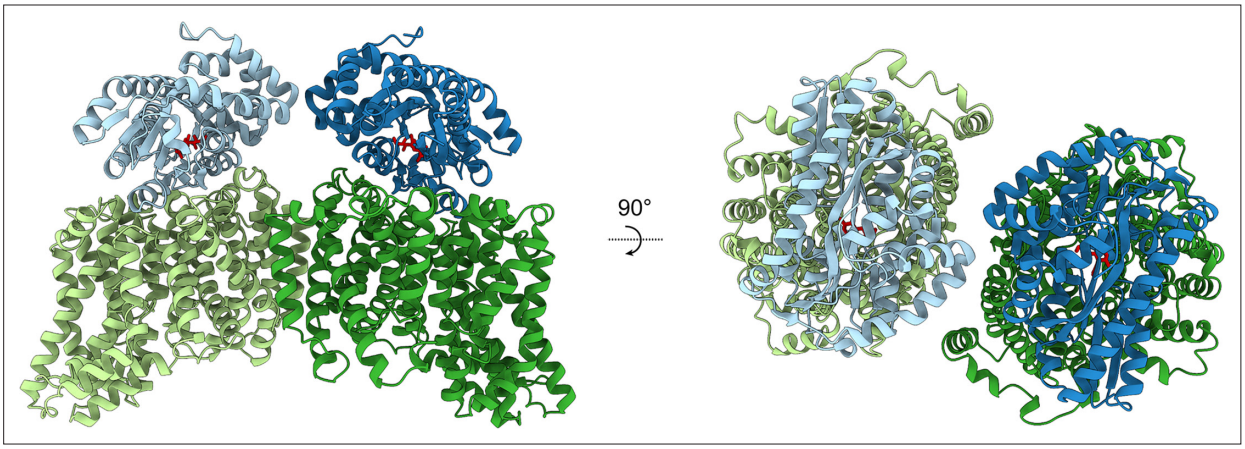

Figure 6—figure supplement 2. Modelling the *Hi*SiaPQM complex. AlphaFold2 was used to model the complex of two *Hi*SiaP monomers (PDB: 3B50) bound to the parallel *Hi*SiaQM dimer from this work (PDB: 8THI). The *Hi*SiaQM monomers are shown in two shades of green and the *Hi*SiaP monomers (ligand bound, closed form) are shown in two shades of blue. Neu5Ac bound to *Hi*SiaP (red sticks) is positioned directly over top of the interface between the scaffold and transport domains of each *Hi*SiaQM monomer. The predicted binding mode of the complex allows for the formation of two complete tripartite *Hi*SiaPQM systems without significant steric clashes.

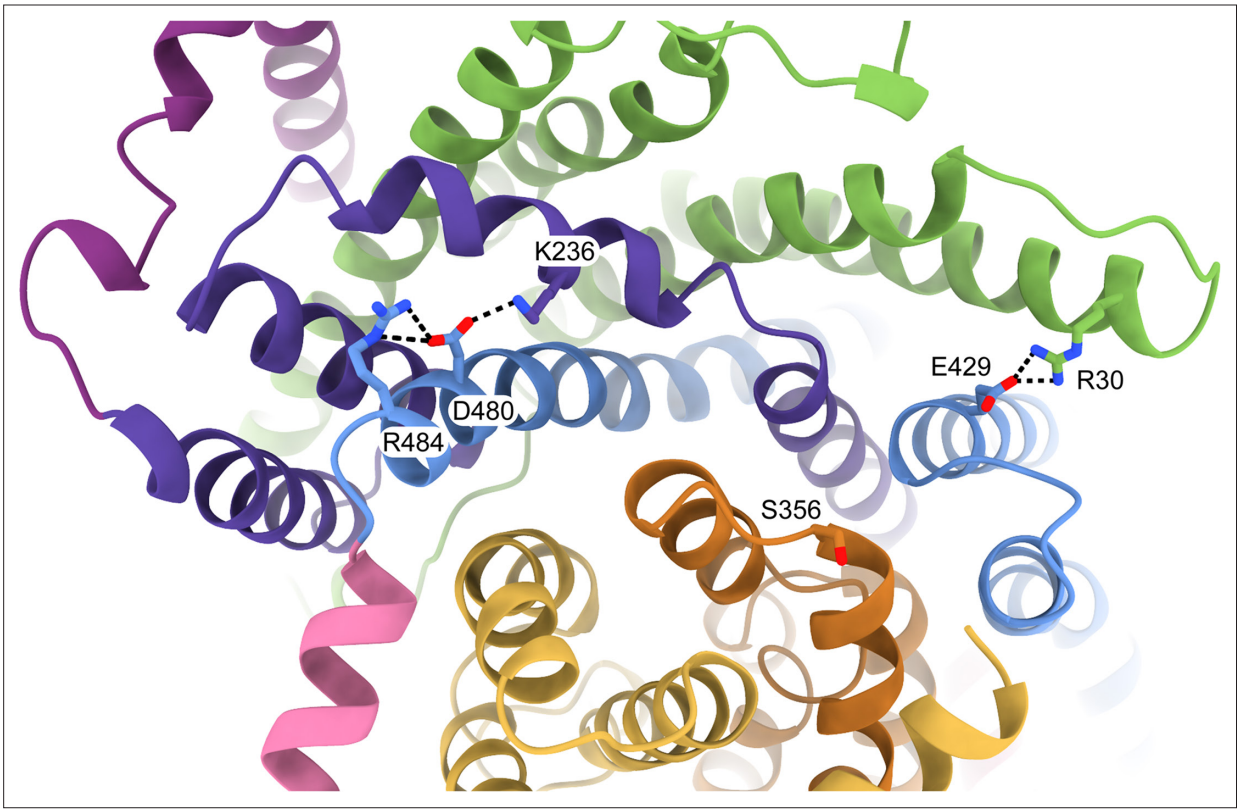

Figure 6—figure supplement 3. Residues involved in scaffold stabilisation and the interaction with SiaP. The resolution of the *Hi*SiaQM structure (coloured as in ***Figure 2c***) shows the positions of R30, S356, E429, and R484 as viewed from the periplasm. R30 (SiaQ, helix 1) forms a salt bridge with E429 (SiaM, helix 8) to connect two helices of the scaffold and SiaQ and SiaM. S356 is located on the loop between helices 5b and 6 of SiaM in the transport domain. R484 (SiaM, helix 9a) forms a salt bridge with D480 (SiaM, helix 9a), which interacts with K236 (SiaM, helix 3a) to connect two helices of the scaffold.

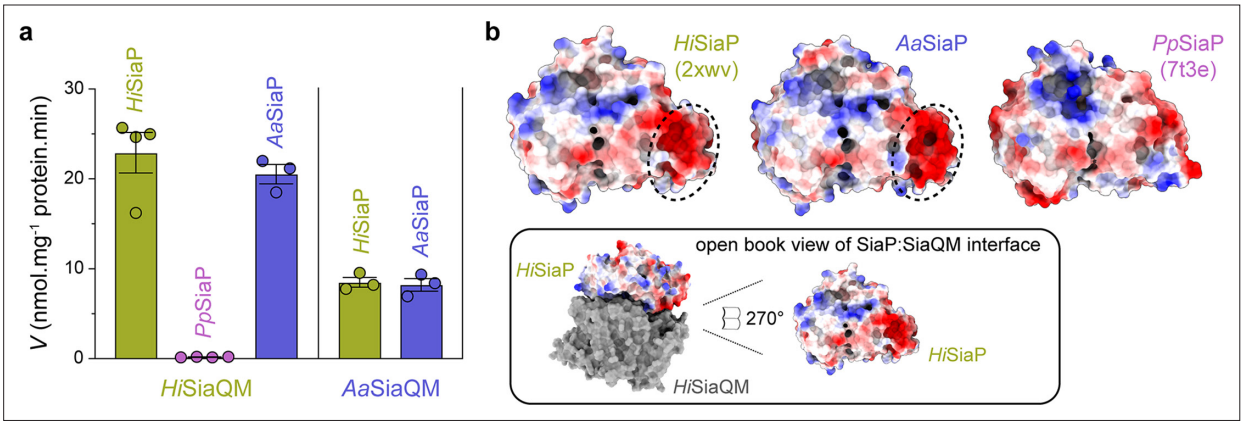

Figure 7. Subunit substitution transport assays. (**a**) Transport was measured with subunit substitution of *Hi*SiaPQM with the fused SiaPQM from *A. actinomycetemcomitans* (*Aa*) and the non-fused SiaPQM from *P. profundum* (*Pp*). Transport activity was measured in the presence of a membrane potential and a Na^+ gradient. The mean activity is shown as bars with SEM error from at least three technical replicates (n = 3 or 4). (**b**) Electrostatic surface comparison of the putative SiaQM interaction surfaces of *Hi*SiaP, *Aa*SiaP and *Pp*SiaP. The SiaP proteins of the two fused systems have a greater area of negatively charged residues (red, circled) at the N-terminal lobe than in the non-fused system.